Initial Excited-state Structural Dynamics of Uridine from Resonance Raman Spectroscopy

Swaroop Sasidharanpillai[+] *Steve P. Dempster and Glen R. Loppnow*[*]

[+]Current address: Department of Chemistry, University of Guelph, Guelph, ON, CANADA N1G2W1

Department of Chemistry, University of Alberta, Edmonton, AB CANADA T6G 2G2

KEYWORDS: Initial excited-state structural dynamics, resonance Raman spectroscopy, uracil, uridine.

ABSTRACT: The effect of the N1 ribose sugar on the initial excited-state structural dynamics of uridine is explored with ultraviolet resonance Raman spectroscopy. Excited-state slopes and broadening parameters were obtained by simulating the resonance Raman excitation profiles and absorption spectrum using a self-consistent, time-dependent formalism. The initial excited-state structural dynamics of uridine look similar to those of uracil, in terms of the distribution of percentage of reorganization energy along different modes, but there is an overall decrease in the excited-state slopes along most of the modes in uridine compared to uracil. Only about 30% of the total initial reorganization energy in both uracil and uridine are oriented along the photochemically reactive co-ordinates. The results are also compared to thymine and thymidine, which show similar results. These differences between thymine/thymidine and

uracil/uridine are examined and the possible effect on the resulting differences in photochemistry is discussed.

INTRODUCTION

Deoxyribonucleic acid (DNA) and ribonucleic acid (RNA) are polymeric genetic material and are made of purine (adenine and guanine) and pyrimidine (cytosine, thymine and uracil) nucleobases connected via a sugar-phosphate backbone[1]. The sugar in DNA is deoxyribose and it is ribose in RNA. Adenine, guanine and cytosine are nucleobases found in both DNA and RNA, while thymine is only found in DNA and uracil only in RNA[1]. The only difference between thymine and uracil (Scheme 1) is the presence of a methyl group at the C5 position of thymine instead of the hydrogen at that position in uracil.

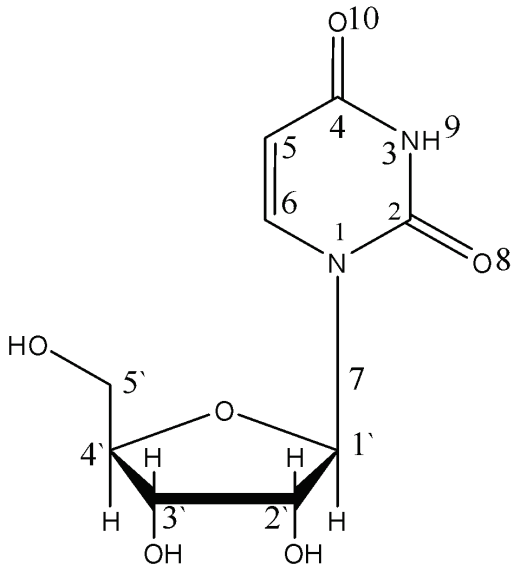

Scheme 1: Structure of 1-β-D-ribofuranosyluracil (uridine).

2'-deoxythymidine is the most photochemically active nucleoside in DNA and uridine is the same in RNA[2]. Thymine forms the cyclobutyl pyrimidine dimer (CPD) as the major photoproduct upon UV irradiation, whereas the photohydrate is the major photoproduct in uracil[2-4]. So the interest in the excited-state dynamics of uracil, thymine and their derivatives stems from the difference in photochemistry despite the similarity in structure of these two nucleobases[2-4].

Much work has been done on the excited-state *electronic* dynamics of nucleobases and nucleotides[5-15]. The excited electronic state of uracil decays at much faster rate (<100 fs) compared to thymine (540 fs)[5,6]. The difference in the excited-state electronic dynamics has been attributed to the mixing of an nπ* state into the final wavefunction in the relaxation process in uracil[7,8]. The excited-state lifetimes of thymine, thymidine and thymidine monophosphate were found to be 0.58, 0.69 and 1.10 ps[9] and for the adenine analogue, they are 1.3, 1.9 and 2.1 ps[10], respectively. These studies show that the sugar plays a role in the excited-state *electronic* dynamics of the nucleosides. The current state of understanding the excited-state dynamics of DNA and its complexity is studied extensively and reviewed by Middleton, et al.,[9] and more recently by Kleinermanns, et al.[11]. The base paring and H-bonding in the G-C base pair decreases the excited-state lifetime and the excited-state lifetimes of single-stranded and double-stranded DNA and are found to be orders of magnitude longer in DNA than in the isolated nucleotides[9]. Also, the excited-state dynamics of nucleosides and nucleotides show a slower decay compared to the corresponding nucleobases[7].

Probing the initial excited-state structural dynamics of the nucleobases will provide insight into the nature of the excited-state potential energy surface near the Franck-Condon

region. Resonance enhancement with the photochemically-relevant excited state can be achieved by laser excitation of the molecule in that electronic absorption region, thereby providing excited-state potential energy surface characteristics of the vibrational modes coupled to the electronic transition. For example, the intensities of the resonance Raman peaks are proportional to the slopes of the excited-state potential energy surface along each vibrational coordinate. The power of resonance Raman spectroscopy to probe the initial excited-state structural dynamics of the molecules has been exploited by Loppnow, et al. in studying thymine, uracil and their derivatives[16-21]. The initial excited-state structural dynamics of uracil in the photochemically-relevant excited state is mostly directed along C5H and C6H bending modes,[16] whereas it is oriented along the C=C stretching mode in thymine[17].

The effect of N1 substitution on initial excited-state structural dynamics in nucleobases has been studied previously. In thymine, the presence of the sugar doesn't change the relative magnitudes of the excited-state potential energy slopes at the Franck-Condon region, but does decrease the overall initial excited-state structural dynamics[16,18]. The observed decrease in the initial excited-state dynamics has been attributed to the presence of less steep excited-state potential energy surfaces and a shift in the potential energy surface at the Frank-Condon region in nucleosides[18]. The initial excited-state structural dynamics of 2'-deoxyguanosine[22] and 9-methyladenine[23] were studied and are consistent with their resulting photochemistry for corresponding nucleobases. Adenine and guanosine nucleobases are not as photochemically active as the pyrimidine nucleobases, and the resonance Raman intensities and resulting initial excited-state structural dynamics of their respective nucleosides are also smaller than those of the pyrimidines, further suggesting a positive correlation between steepness of the potential energy

surface and photochemical quantum yield. The initial excited-state structural dynamics of uracil[17] and some of its derivatives[19-21] are well understood, so it is important to explore the effect of sugar on the initial excited-state structural dynamics of uracil. Onidas et al.[24] looked at the difference in fluorescence lifetime and fluorescence anisotropy decays for some of the nucleosides and corresponding nucleotides and found that there is no difference between purine nucleoside and nucleotides, but the lifetime and anisotropy increases with the presence of the phosphate group in the pyrimidine nucleotides. The initial excited-state structural dynamics of uracil has been studied previously, but no such studies on the uracil nucleoside or nucleotide have been reported.

In this paper, we have studied the effect of ribose sugar on the initial excited-state structural dynamics of uracil and here report the initial excited-state structural dynamics of uridine (Scheme 1) using resonance Raman spectroscopy. The results discussed here demonstrate that the presence of the sugar on N1 doesn't affect the initial excited-state structural dynamics of the uracil nucleobase, in contrast to what is observed for thymine. The experimental results will be discussed in the light of known photochemistry of DNA and will be compared to the photochemistry of thymine. The results show that the initial excited-state structural dynamics of uridine is primary oriented along the pyramidalization coordinate as in uracil and the result obtained here are compared with that of thymine and thymidine to better understand the excited-state dynamics difference between the two pyrimidine nucleosides.

EXPERIMENTAL

Uridine (1-β-D-ribofuranosyluracil, Sigma-Aldrich, Oakville, Ontario), and sodium sulphate and sodium nitrate (99%, EMD Chemicals Inc., Gibbstown, NJ) were used without any further purification. Solutions were prepared with nanopure water from a Barnstead water filtration system (Boston, MA). The concentration of uridine was 3-5 mM and the sodium sulphate internal standard concentration was 0.3 M.

The laser wavelengths for resonance Raman excitation were obtained from a picosecond mode-locked, Ti:sapphire laser (Coherent, Santa Clara, CA) pumped by a doubled, continuous-wave, solid-state, diode-pumped Nd:YAG laser (Coherent, Santa Clara, CA). The output of the tunable Ti:sapphire laser was doubled with a lithium triborate (LBO) crystal (Inrad, Northvale, NJ) followed by third harmonic generation using a β-barium borate (BBO) crystal (Inrad, Northvale, NJ) in a harmonic generator (Inrad, Northvale, NJ) to get 244, 257, 266, 275 and 290 nm excitation wavelengths. The power of the laser beam was typically 1-25 mW depending upon the excitation wavelength. The third harmonic output from the harmonic generator was spherically focused onto an open stream of flowing solution in a 135º back-scattering geometry. The resonance Raman scattering was focused into a double-grating spectrometer (Spex Industries, Metuchen, NJ) with a water-cooled diode array detector. All resonance Raman spectral measurements were done in triplicate. Resonance Raman frequencies for uridine reported here are accurate to ±5-7 cm^{-1}. The frequencies were calibrated by measuring the Raman scattering of the solvents with known frequencies (acetonitrile, carbon tetrachloride, cyclohexane, dimethylsulfoxide, ethanol and methanol). The actual uridine concentration during the experiment was monitored by measuring the absorption spectrum before and after each

resonance Raman experiment, using a diode array absorption spectrometer (Hewlett-Packard 8452, Sunnyvale, CA).

The overtone and combination bands at 257 nm for uridine were recorded using a UV Raman microscope (Renishaw, Chicago, IL) as described previously[16]. A solution of 5 mM uridine and 0.3 M nitrate in a small beaker was constantly moved by using a translation stage to minimize photodegradation of the sample. The 1332 cm^{-1} vibration of diamond was used to calibrate the frequencies. The resonance Raman spectra in the overtone and combination band region were recorded with three sets of fresh samples.

The absolute resonance Raman cross-sections were calculated from the integrated band intensities using the following equation.

$$\left(\frac{d\sigma_R}{d}\right)_{Uridine} = \left(\frac{d\sigma_R}{d}\right)_{IS} \cdot \frac{I_{Urdine,}}{I_{IS}} \cdot \frac{[IS]}{[Uridine]} \cdot \frac{L_{Urdine}}{L_{IS}} \cdot SA \qquad (1)$$

Where $d\sigma_R/d\Omega$ is the differential resonance Raman cross-section of the vibrational mode, I_{Urdine} and I_{IS} are the integrated band intensities of the uridine and internal standard, respectively, [IS] and [Uridine] are the concentrations of the internal standard and uridine, respectively, $L_{Uridine}$ and L_{IS} are the standard lamp efficiency at the uridine and internal standard vibrational frequencies, respectively, and SA is the differential self-absorption of the resonance Raman scattered light at the uridine and internal standard vibrational frequencies. Details of converting the resonance Raman intensities to differential resonance Raman cross-section have been described previously.[25-27] The internal standard resonance Raman differential cross-sections for sulfate used

for the calculations were 3.54 x 10^{-12}, 2.71 x 10^{-12}, 2.28 x 10^{-12}, 1.93 x 10^{-12} and 1.49 x 10^{-12} Å^2 molecule^{-1} sr^{-1} at 244, 257, 266, 275 and 290 nm, respectively.

Resonance Raman structural dynamics. The absorption spectrum and resonance Raman differential cross-sections as a function of excitation wavelength (excitation profiles) for uridine were simulated with a time-dependent formalism as described previously[26-28].

$$\sigma_A(E_L) = \frac{4\pi E_L e^2 M^2}{6\hbar^2 cn} \int_0^\infty dE_0 H(E_0) \int_{-\infty}^{\infty} dt \langle i | i(t) \rangle \exp\{\frac{i(E_L + \varepsilon_i)t}{\hbar}\} G(t)$$

$$\sigma_R(E_L) = \frac{8\pi E_s^3 E_L e^4 M^4}{9\hbar^6 c^4} \int_0^\infty dE_0 H(E_0) | \int_0^\infty dt \langle f | i(t) \rangle \exp\{\frac{i(E_L + \varepsilon_i)t}{\hbar}\} G(t) |^2$$

(2)

(3)

where E_L and E_S are the energies of the incident and scattered photons, respectively, M is the transition length, *n* is the refractive index, ε_i is the energy of the initial vibrational state, |i> and |f> are the initial and final vibrational wavefunctions in the Raman scattering process, respectively, $H(E_0)$ is a normalized inhomogeneous distribution of the zero-zero energies around an average zero-zero energy ($\bar{E}_0$), |i(t)> is the initial ground vibrational wavefunction propagated on the excited-state potential energy surface, and G(t) is the homogeneous linewidth function, which represents the dynamics of chromophore-solvent coupling within the high-temperature limit of the Brownian oscillator model[29]. Within the harmonic oscillator approximation, the

<i|i(t)> and <f|i(t)> overlaps depend only on the slopes ($\beta/\hbar$) of the excited-state potential energy surface at the ground-state equilibrium geometry along each normal mode of vibration. The implementation of these equations have been described in detail previously[26-29]. The self-consistent simulation of the absorption spectrum and resonance Raman excitation profiles has been performed as previously described[16]. For the analysis, the parameters were adjusted to get good agreement between the experimental and simulated absorption spectra and resonance Raman excitation profiles. The overtones and combination bands were used as additional constraints to optimize the parameters.

RESULTS

Figure 1 shows the resonance Raman spectra of uridine excited at different laser wavelengths (290, 275, 266, 257 and 244 nm) within the 260 nm absorption band. Peaks are observed at 627, 781, 1231, 1393, 1473, 1563, 1629 and 1678 cm^{-1}. The relative intensities and frequencies of the different peaks remain mostly the same at different excitation wavelengths indicating that the resonance enhancement is from a single electronic transition within the 260 nm absorption band. However, some differences are observed in the relative intensities of the 1629 and 1657 cm^{-1} peaks at 257 and 244 nm, suggesting some pre-resonance or resonance enhancement may be occuring in one or more of those peaks from a higher-lying excited state. The higher-lying excited states of uracil carry more $\pi\sigma^*$ and $\sigma\sigma^*$ character, which may lead to more resonance Raman intensity in the carbon-carbon stretches[30,31]. The resonance Raman spectrum of uridine is similar to that of uracil (Figure 2)[16], with some slightly altered frequencies, so the peak assignment and potential energy distributions are based on the uracil

peak assignments (Table 1). For the assignments of resonance Raman peaks which are absent in uracil (e.g. 1473 cm^{-1}), the uridine

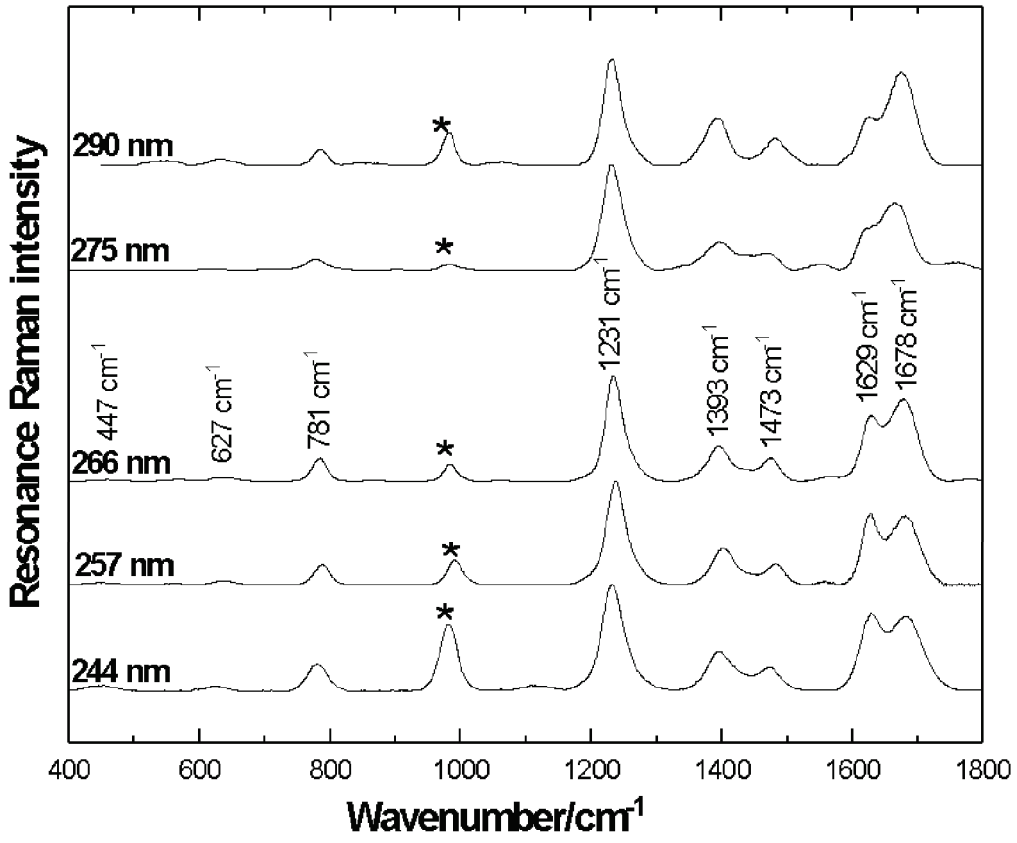

Figure 1: Resonance Raman spectra of 1-β-D-ribofuranosyluracil (uridine) excited at different wavelengths throughout the 260 nm absorption band. The concentration of uridine was ~5 mM and that of the sulfate internal standard was 0.3 M. The internal standard peak is denoted by an asterisk (*). All the spectra are normalized with respect to the 1231 cm^{-1} peak.

vibrational spectral assignments by Leulliot et al.[32] were used.

The two most intense bands are observed at 1231 (hydrogen bends + ring stretches) and 1678 cm^{-1} (C4 carbonyl stretch) which are observed at 1235 and 1664 cm^{-1}, respectively, in uracil. The peak at 1393 cm^{-1} is assigned to a ring stretch and the C5=C6 stretching is observed at 1629 cm^{-1} similar to uracil. The 447 and 1473 cm^{-1} peaks were assigned from the theoretical calculations of Leulliot, et al., and are assigned to the C5H wag + N1C6 torsion and the N1C6 stretch + C5C6H bend, respectively[30]. A complete mode description and the potential energy distribution for uridine and uracil are given in Tables 1 and 2, respectively.

Table 1: Harmonic parameter for 1-β -D-ribofuranosyluracil**.**

Mode[a] (cm^{-1})	Mode Assignment[b]	β /ħ[c] (cm^{-1})
447	$\omega(C_5H_{11})$ [17] , τ (N_1C_6) [17]	50
627	Ring def 3 [32], be(C_2O_8) [-23], be(C_4O_{10}) [-18], ν (C_4C_5) [-6], ν (C_6N_1) [6]	80
781	ν (C_4C_5) [28], ν (N_1C_2) [19], Ring def 1 [-13], ν (N_3C_4) [10], Ring def 3 [-7], ν (C_2N_3) [6], ν (C_6N_1) [6]	140
1231	be(C_5H_{11}) [33], be(C_6H_{12}) [18], ν (C_6N_1) [-15],be(N_1H_7) [-10], ν (N_3C_4) [7], ν (N_1C_2) [5]	430
1393	ν (C_2N_3) [18], be(N_3H_9) [17], ν (N_1C_2) [-15], be(C_5H_{11}) [13], be(C_6H_{12}) [-12], ν (C_5C_6) [-8], be(C_4O_{10}) [5]	280
1473	ν (N_1C_6) [17],be(C_5C_6H) [11]	220
1629	ν (C_5C_6) [61], be(C_6H_{12}) [-14], ν (C_6N_1) [-8]	350
1678	ν (C_4O_{10}) [71], ν (C_4C_5) [-8], Ring def 2 [5]	500

[a]Frequencies listed here are experimental frequencies. [b]Abbreviations: ν - stretching, def - deformation, ω - out of plane wagging, τ - torsion, be - in-plane bending. Numbers in square parentheses are the potential energy distribution (P.E.D.) contribution of that internal coordinate to the normal mode. Assignments are from ref. 16 and 32. [c]Slopes of the excited-state potential energy surface at the Franck–Condon geometry (β/ħ) were obtained by fitting the experimental resonance Raman cross-sections and absorption spectrum with the following parameters in Equations 2 and 3: temperature, T = 298 K, zero-zero energy, E_0 = 37150 cm^{-1}, Gaussian homogeneous linewidth, Γ_G = 1150 cm^{-1}, inhomogeneous linewidth, θ = 1220 cm^{-1}, transition length, M = 0.71 Å, and Brownian oscillator line shape, κ = Λ/D = 0.1.

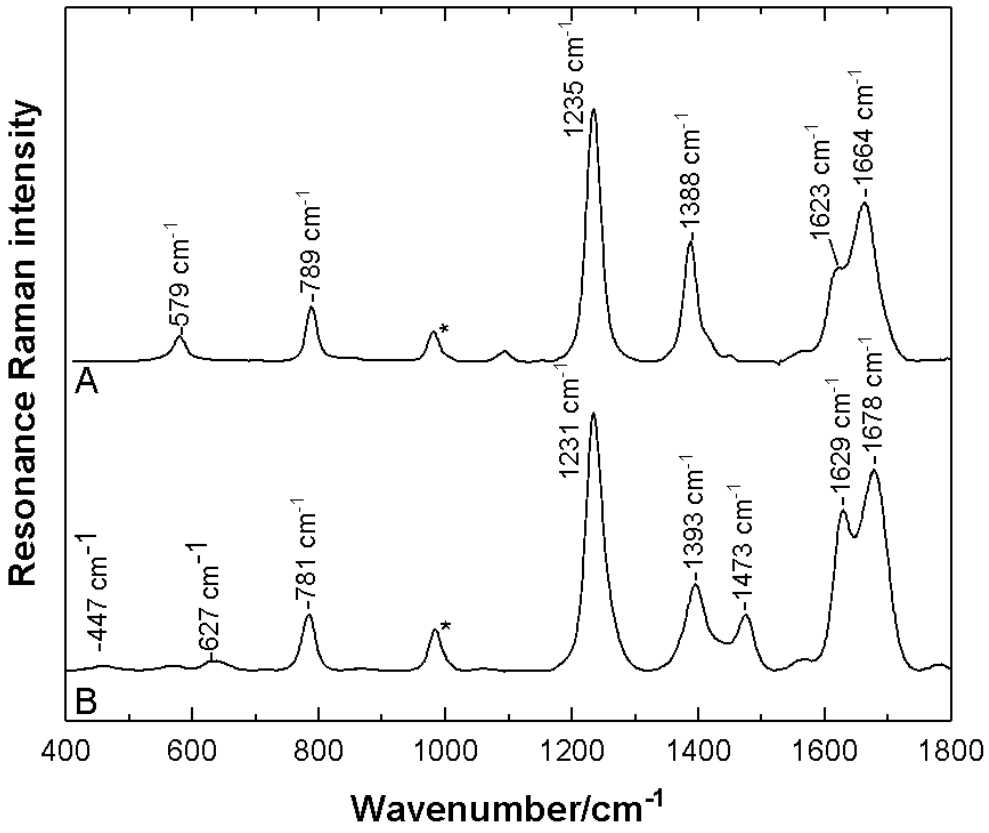

Figure 2. Comparison the resonance Raman spectra of 3-5 mM uracil (A) and uridine (B) solutions each containing 0.3 M nitrate excited at 266 nm.

The potential energy distributions of both uridine and uracil reflect the resonance Raman spectra shown in Figure 2. Comparison of Tables 1 and 2 shows that the excited-state slope ($\beta/\hbar$) is higher for each mode in uracil compared to the similar mode in uridine. There are more

resonance Raman peaks in uridine compared to uracil, which is evident from Figure 2 and not unexpected, given that uridine is a larger molecule with more atoms.

Table 2: Harmonic parameter for uracil*

Mode (cm^{-1})	Mode Assignment	β/ħ (cm^{-1})
579	Ring def 3 [32], be(C_2O_8) [-23], be(C_4O_{10}) [-18], ν (C_4C_5) [-6], ν (C_6N_1) [6]	270
789	ν (C_4C_5) [28], ν (N_1C_2) [19], Ring def 1 [-13], ν (N_3C_4) [10], Ring def 3 [-7], ν (C_2N_3) [6], ν (C_6N_1) [6]	380
1235	be(C_5H_{11}) [33], be(C_6H_{12}) [18], ν (C_6N_1) [-15], be(N_1H_7) [10], ν (N_3C_4) [7], ν (N_1C_2) [5]	910
1388	ν (C_2N_3) [18], be(N_3H_9) [17], ν (N_1C_2) [-15], be(C_5H_{11}) [13], be(C_6H_{12}) [-12], ν (C_5C_6) [-8], be(C_4O_{10}) [5]	620
1623	ν (C_5C_6) [61], be(C_6H_{12}) [-14], ν (C_6N_1) [-8]	490
1664	ν (C_4O_{10}) [71], ν (C_4C_5) [-8], Ring def 2 [5]	1000

*Data from ref. 16: temperature, T = 298 K, zero-zero energy, E_0 = 36500 cm^{-1}, Gaussian homogeneous linewidth, Γ_G = 1450 cm^{-1}, inhomogeneous linewidth, θ = 1000 cm^{-1}, transition length, M = 0.65 Å, and Brownian oscillator line shape, κ = Λ/D = 0.1.

Figure 3 shows the experimental and simulated absorption spectra, and Figure 4 shows the experimental and simulated resonance Raman excitation profiles of uridine. The absorption spectrum and resonance Raman excitation profiles (RREPs) were simulated by adjusting the parameters in Equations 2 and 3, respectively, to get the best agreement between the experimental and simulated absorption. Differences between the experimental and the calculated absorption spectra at energies above 38000 cm^{-1} is due to the fact that the higher energy electronic absorptions are not modeled in the simulation but may still contribute to the experimental absorption spectrum. The discrepancy between the experimental and simulated absorption spectrum in the region 34,500-37,500 cm^{-1} is likely due to a n π^* transition, which is perhaps gaining oscillator strength via vibronic coupling with the sugar.

The simulated resonance Raman excitation profiles fit well with the experimentally measured resonance Raman cross-sections well, except for the higher experimental resonance Raman cross-section at 275 nm (36,363 cm^{-1}) excitation for some modes. In a different model, we have attempted to fit the high cross-section at 275 nm with larger slopes along each mode. This model, with larger excited-state slopes, could not account for the observed intensities of the overtones and combination bands, and was not pursued any further. The modes at 275 nm excitation may also be resonant with the somewhat enhanced n π * state, but expected changes in relative intensity at this excitation wavelength are not observed. The relative intensities of the

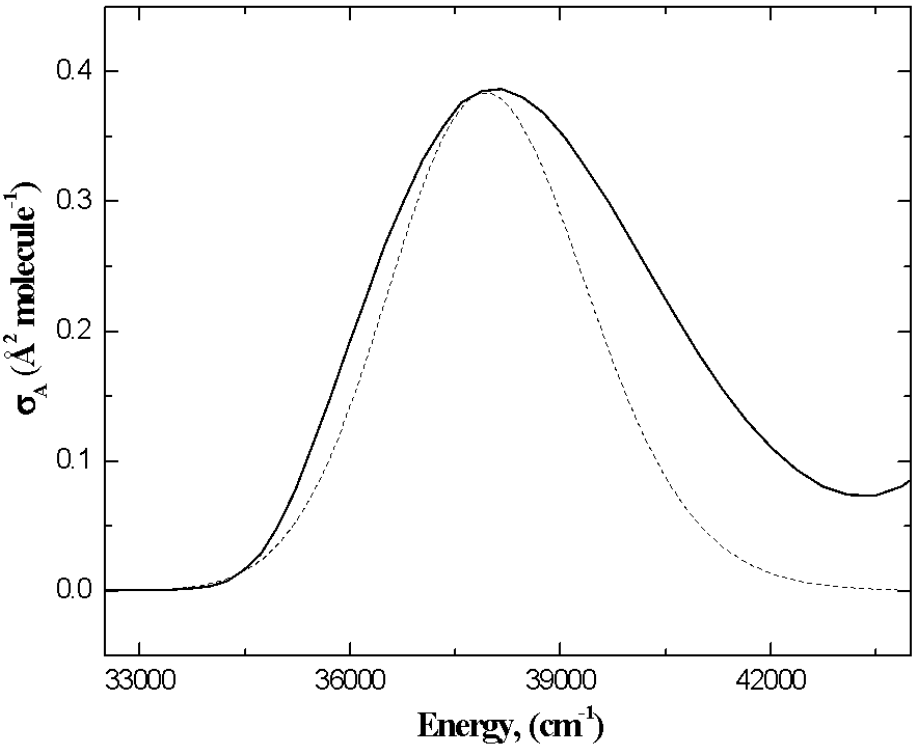

Figure 3: Calculated (dashed line) and experimental (solid line) absorption spectrum of uridine. The simulated absorption spectrum was generated using Equation 2 and the parameters of Table

1. The difference between the experimental and simulated spectra at energies higher than 38000 cm^{-1} is due to other higher energy transitions which are not modeled in the equation.

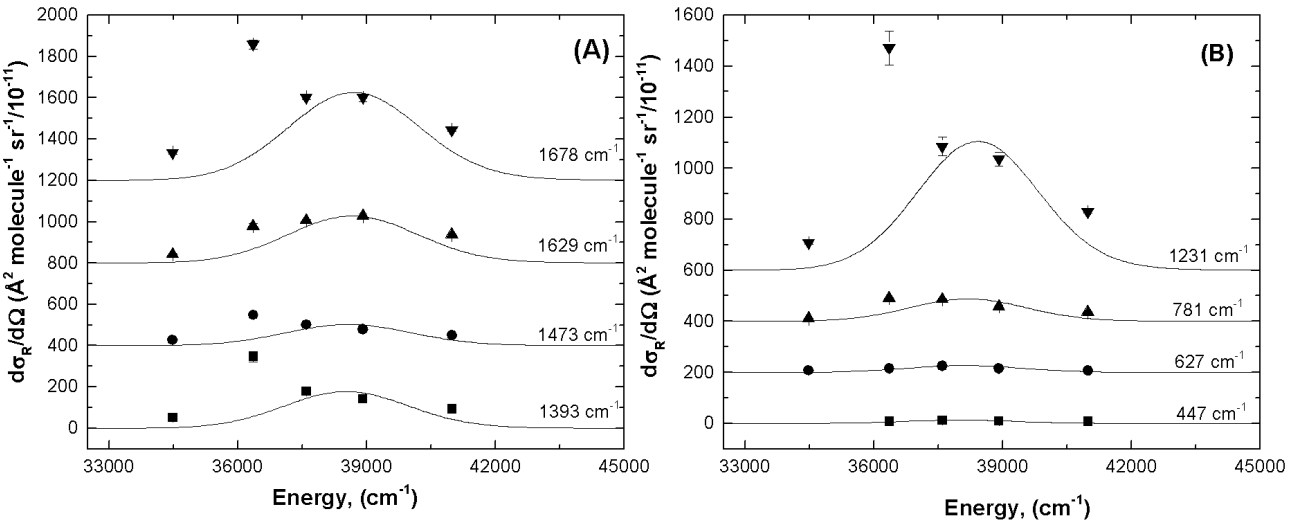

Figure 4: Experimental (points) and calculated resonance Raman excitation profiles (solid line) for uridine at high wavenumbers (A) and low wavenumbers (B). The excitation profiles were calculated using Equation 3 and the parameters of Table 1.

resonance Raman peaks in Figure 1 are proportional to the different RREPs. The goodness of the fits indicates that the excited-state parameters obtained from the simulation are able to reproduce the absorption spectrum and the resonance Raman excitation profile accurately.

The overtones and combination bands between 1800 and 3000 cm^{-1} were also measured at 257 nm in an effort to better constrain the parameters used for the simulation of the absorption spectrum and the fundamental resonance Raman excitation profiles. The overtone and combination bands above 3000 cm^{-1} were obscured by the broad O-H stretching vibrations of water. Table 3 tabulates the experimental and predicted overtones and combination bands for uridine. Most of the calculated overtone and combination band intensities are in agreement with the observed intensities within the experimental error, except for the 2015, 2632 and 2696 cm^{-1} bands. These bands are all higher in the simulated cross-sections and share the 1231 cm^{-1} mode in common, suggesting that the derived excited-state slope for this mode may be too low. However, no other set of parameters better fit the experimental absorption spectrum and all the other excitation profiles. The higher degrees of error in the experimental overtone and combination band cross-sections compared to the fundamental cross-sections are due to both their lower intensity and additional observed imprecision arising from focus-dependent intensities in the Raman microscope. The agreement between the experimental and calculated cross-sections ensures the accuracy of the parameters used to simulate the absorption spectrum and resonance Raman excitation profiles.

Table 3: Experimental and calculated resonance Raman cross-sections for overtone and combination bands of uridine.*

Mode (cm^{-1})	Mode assignment	$d\sigma_{experimental}/d\Omega$ ($Å^2$ molecule^{-1} $sr^{-1}/10^{-11}$)	$d\sigma_{calculated}/d\Omega$ ($Å^2$ molecule^{-1} $sr^{-1}/10^{-11}$)
2015	627+1393, 781+1231	8±2	15
2093	447+1629, 446+1678, 627+1473	3±1	2
2412	781+1628	3±1	5
2464	2X1231, 781+1678	5±2	3
2632	1231+1393	20±4	45
2696	1231+1473	3±1	13
2866	1231+1628, 1393+1473	5±2	5
2904	1231+1678	6±2	5

*Frequencies listed are experimental frequencies. Cross-sections were calculated using Equation 3 and the parameters in Table 1. Experimental cross-sections were calculated from the resonance Raman spectra of overtone and combination bands of uridine at 257 nm.

Table 4 compares the electronic and broadening parameters of uracil and uridine. All the parameters are slightly higher for uridine compared to uracil, except for the homogeneous broadening, Γ_G. However, the total broadening is the same, suggesting that all the electronic and broadening parameters are similar for uracil and uridine, consistent with what was observed for thymine and thymidine[18].

Table 4: Comparison of the harmonic parameters of uracil and uridine.

	Uracil[a]	Uridine
E_0 (cm^{-1})	36500	37150
M (Å)	0.65	0.71
θ (cm^{-1})	1000	1220
Γ_G (cm^{-1})	1450	1150

E_0 is the zero-zero energy, M is the transition length, θ is the inhomogeneous linewidth and Γ_G is the homogeneous linewidth. [a]The harmonic parameters of uracil were obtained from reference 16.

DISCUSSION

Considering the UV-induced photochemistry of uracil, which forms the photohydrate (major photoproduct) and cyclobutyl photodimer (minor photoproduct), lengthening of the C5=C6 and bending of the C5-H and C6-H bonds are expected to be the primary initial excited-state structural dynamics, if the excited-state photochemistry maps along the primary reaction coordinates well. Intense resonance Raman peaks along the C5=C6 stretching and the C5-H and C6-H bending modes indicates that the initial excited-state structural dynamics do lie along these photochemically active coordinates.

The results presented above show that uridine has similar resonance Raman peak frequencies to those of uracil, indicating that the presence of the sugar doesn't change the ground-state vibrational structure of the nucleobase[16,30,33,34]. Also, the fact that the *relative* resonance Raman intensities in the spectra of uracil and uridine are the same indicates that the *relative proportion* of initial excited-state structural dynamics along each mode are the same in the two. The most intense band in uridine is the 1231 cm^{-1} mode, which is assigned to the C5-H and C6-H in-plane bending modes coupled to other stretches and bends throughout the ring and observed at 1235 cm^{-1} in uracil. This large intensity for the C-H bending mode is expected, as the photohydrate is the major photoproduct upon UV-irradiation and this mode projects along the photochemical reaction coordinate well[2]. The second most intense peak is the 1678 cm^{-1} mode, which is seen at 1664 cm^{-1} in uracil, and is mainly due to the C4=O10 stretch. This mode doesn't lie along any photochemically active coordinates. The large initial excited-state structural dynamics along this mode which does not have any projection on the photochemical reaction coordinate might be one reason for the reduced photochemical activity of uracil compared to

thymine. The other two intense modes at 1393 and 1629 cm^{-1} have projection on the C5H and C6H bends and C5C6 stretching photochemically active coordinates. The presence of a new peak at 1472 cm^{-1} compared to uracil, which has a small projection on the photochemical active coordinate, might serve to diffuse the total amount of initial excited-state structural dynamics oriented along the photochemical active coordinate into other coordinates, compared to uracil.

One of the most important outcomes of the initial excited-state structural dynamics comparison between uracil and uridine is the total lowering of the initial excited-state structural dynamics upon the addition of the sugar at N1, even though the pattern of initial excited-state structural dynamics in the two is similar. Also, the initial excited-state structural dynamics are lower for each internal coordinate, although the total percentage of initial excited-state structural dynamics projected on the photochemical active coordinates remains the same for uridine with respect to uracil (see Tables 1, 2 and 5). The presence of the sugar thus acts as a mean of increasing the amount of dissipative motions and decreasing the slope of the overall potential energy surface at the Franck-Condon region in the molecule, thereby enhancing the photochemical stability. A flatter excited-state potential energy surface is well supported by the longer excited-state lifetime in the nucleosides compared to the nucleobases[9,24].

Comparison of the pyrimidine base initial excited-state structural dynamics. We have used a method for comparing the initial excited-state structural dynamics[35] of different molecules by comparing the total amount of structural reorganizational energy distributed along each of the different internal coordinates. We use that here to compare the initial excited-state structural dynamics of uracil, uridine, thymine, and thymidine. The following equation was used

to calculate the percentage of reorganization energy distributed along a particular internal coordinate[35]

$$\%\ reorganization\ energy = \frac{\sum_{j=1}^{n}\left\{\left(\frac{\left(\frac{\beta}{\hbar}\right)^2}{2\bar{\nu}}\right)_j C_{ij}\right\}}{\sum_{j=1}^{n}\left(\frac{\left(\frac{\beta}{\hbar}\right)^2}{2\bar{\nu}}\right)_j} X\ 100\% \qquad (4)$$

where $\frac{\left(\frac{\beta}{\hbar}\right)^2}{2\bar{\nu}}$ is each normal mode's reorganization energy, $\bar{\nu}$ is the vibrational wavenumber (cm^{-1}), c_{ij} is the percentage contribution of the i^{th} internal coordinate to the j^{th} normal mode, and n is the total number of observed normal modes. Thus, the total fraction of reorganization energy along a particular internal coordinate is calculated by summing up the individual reorganization along that particular internal coordinate and dividing by the total reorganization energy. For example, using the data in Table 1, we find a total reorganization energy for uridine of 250 cm^{-1}, of which 10% of that (25 cm^{-1}) is along the C5=C6 stretch in the 1393 (8%) and 1629 (61%) cm^{-1} modes. This calculation assumes that unobserved mode contributions are insignificant.

The mode-to-mode comparison of the distribution of reorganization energies in Table 5 shows that the addition of sugar to uracil doesn't affect the distribution of reorganization energies

along any of the internal coordinates in an appreciable amount. A similar effect is observed in thymine as well upon addition of the sugar to N1. It is worth noting in uridine that the reorganization energy along the C5=C6 stretching mode increases slightly and that energy along the C5+C6 bending mode decreases by a small amount upon addition of the ribosyl sugar at N1. These results all indicate that the difference in the individual initial excited-state structural

dynamics for uracil and uridine are small, but that the overall dynamics (from the individual excited-state slopes) are much smaller upon addition of the ribosyl sugar at N1 on uracil.

Table 5: Comparison of reorganization energies along different internal coordinates for thymine, thymidine, uracil and uridine.*

	Ring str	Ring def	C4O10 str	C5C6 str	C5 bend	C6 bend	C5+C6 bend	Activity along reactive coordinates
T	16%	5%	0%	24%	8%	15%	23%	47%
Td	19%	6%	0%	27%	8%	16%	24%	51%
U	23%	5%	21%	6%	13%	9%	22%	27%
Ud	20%	3%	21%	10%	11%	9%	20%	30%

*The calculations are done similar to ref. 35 and using Equation 4. 'Str' is stretch, 'T' is thymine, 'Td' is thymidine, 'U' is uracil, and 'Ud' is uridine. The values for thymine and thymidine were calculated from references 17 and 18.

Electronic dynamics and initial excited-state structural dynamics: The evolution of the excited-state potential energy surface upon photon absorption is the initial step in the photochemistry of the compound. In other words, the Franck-Condon geometry on the excited-state is the starting point of the excited-state structural dynamics. These excited-state structural dynamics precede evolution of the excited electronic state via photophysical processes and/or photochemistry. The resonance Raman excitation profile probes only the initial excited-state dynamics near the Franck-Condon region, effectively providing the excited-state potential energy surface slopes along each normal mode at the ground-state molecular geometry. These initial excited-state structural dynamics are necessary to understand the later electronic dynamics.

Even a small difference in the initial excited-state geometry may change the very nature of the excited-state potential energy surface by changing the position and crossing probabilities of conical intersection(s). The comparison of the initial excited-state slopes of uracil, thymine

and their nucleosides shows that they are different[18,33]. There is a decrease in the initial excited-state slopes with the addition of sugar to thymine[18, 36] and uracil. The initial energy along a dissipative mode, the C4O10 stretch, is the same in uracil and uridine indicating that a bigger substitution at N1 is not changing the initial dynamics of the excited-state potential energy surface in uracil. This is similar to the previous resonance Raman excitation studies with uridine monophosphate[30,34]. But when we examine the overall excited-state structural dynamics of uridine along all the vibrational modes, there is a substantial decrease upon the addition of the sugar, which was previously seen with other thymine derivatives as well[18]. This decrease can be attributed to the presence of a larger number of additional vibrational modes in nucleosides compared to nucleobases through which the excited state evolves, effectively flattening out the excited-state potential energy surface along photochemical modes and decreasing the resulting photochemical quantum yield.

On comparing the initial excited-state dynamics of nucleosides of thymine and uracil, it is clear from Table 5 that in uracil and thymine, there is no observable change in the percentage of total excited-state energy oriented along the reactive coordinates with the addition of sugar. So the presence of the sugar affects excited-state motion similarly in uracil and thymine.

Fluorescence up-conversion studies by Gustavsson, et al., show that uracil has an ultra-short excited-state lifetime of around 100 femtoseconds[5,37-40]. C5 pyramidalization is believed to be responsible for this ultrafast decay via a conical intersection between the ground state (S_0) and the excited state ($\pi\pi^*$)[5]. Thus, a small decrease in the reorganization energy proportion along C5 pyramidalization and a net decrease in the overall initial excited-state structural dynamics along all the normal coordinates is consistent with an increase in the

excited-state life time of uridine compared to uracil, since the overall dynamics and time to the conical intersection would be longer with shallower slopes. However, more work needs to be done to completely elucidate the excited-state structural dynamics.

The decrease in homogeneous linewidth in uridine compared to uracil is expected as the homogeneous broadening results mostly from solvent-induced dephasing. This decrease suggests that the sugar may play a role in dephasing the excited-state wavepacket faster, due to its increased interaction with solvent. Similarly, the large inhomogeneous broadening is from a distribution of different E_0 energies. The increase in the inhomogeneous linewidth in uridine compared to uracil may result from the increase in size of the molecule and the subsequent larger distribution of solute-solvent interactions which then lead to a larger distribution of E_0 energies. These results are consistent with the increase in inhomogeneous linewidth observed in going from thymine to thymidine[16,18]. The increased solvent interaction and the resulting dephasing mechanism by water may also change the resulting photochemistry of the nucleosides/nucleotides compared to the nucleobases, consistent with the observed changes in photochemical quantum yield.

CONCLUSIONS

The initial excited-state structural dynamics of 1-β-D-ribofuranosyluracil (uridine) is similar to that of uracil with respect to the percentage of reorganization energy along different modes. However, the overall excited-state slopes are smaller in uridine compared to uracil, suggesting

that the initial excited-state structural dynamics are slower in uridine compared to uracil. This conclusion is consistent with the results found for thymidine compared to thymine.

Corresponding Author

* e-mail: Glen R. Loppnow, glen.loppnow@ualberta.ca

ACKNOWLEDGEMENTS

The authors acknowledge the Natural Science and Engineering Research Council (NSERC) of Canada for financially supporting this work through their Discovery Grants-in-Aid programme.

REFERENCES

1. Lehninger, A. L.; *Biochemistry,* Worth publications, 1975, Vol 2, pp 309-333.
2. Ruzsicska, B. P.; Lemaire, D. G. E. DNA photochemistry. In *CRC Handbook of Organic Photochemistry and Photobiology*; Horspool, W. H., Song, P.-S., Eds.; CRC Press: New York, 1995; pp 1289-1317.
3. Shetlar, M. D.; Basus, V. J. The photochemistry of uracil: A reinvestigation. *Photochem. Photobiol.* **2011**, *87*, 82–102.
4. Cadet, J.; Mouret, S.; Ravanat, J-L.; Douki, T. Photoinduced damage to cellular DNA: Direct and photosensitized reactions. *Photochem. Photobiol.,* **2012**, 88, 1048-1065.
5. Gustavsson, T.; Banyasz, A.; Lazzarotto, E.; Markovitsi, D.; Scalmani, G.; Frisch, M. J.; Barone, V.; Improta, R. Singlet excited-state behavior of uracil and thymine in aqueous

solution: A combined experimental and computational study of 11 uracil derivatives. *J. Am. Chem. Soc*. **2006**, *128*, 607-619.

6. Merchan, M.; Gonzalez-Luque, R.; Climent, T.; Serrano-Andrs, L.; Rodraguez, E.; Reguero, M.; Pelaez, D. Unified model for the ultrafast decay of pyrimidine nucleobases. *J. Phys. Chem. B* **2006**, *110*, 26471-26476.
7. Hare, P. M.; Crespo-Hernandez, C. E.; Kohler, B. Internal conversion to the electronic ground state occurs via two distinct pathways for pyrimidine bases in aqueous solution. *Proc. Natl. Acad. Sci. U.S.A.* **2007**, *104*, 435-440.
8. Barbatti, M.; Aquino, A. J. A.; Szymczak, J. J.; Nachtigallova, D.; Hobza, P.; Lischka, H. Relaxation mechanisms of UV-photoexcited DNA and RNA nucleobases. *Proc. Natl. Acad. Sci. U.S.A*. **2010**, *107*, 21453-21458.
9. Middleton, C. T.; de La Harpe, K.; Su, .C; Law, Y. K.; Crespo-Hernandez, C. E.; Kohler, B. DNA excited-state dynamics: From single bases to the double helix. *Ann. Rev. Phys. Chem*. **2009**, *60*, 217-239.
10. Kwok, W. M.; Ma, C.; Phillips, D. L. Femtosecond time- and wavelength-resolved fluorescence and absorption spectroscopic study of the excited states of adenosine and an adenine oligomer. *J. Am. Chem. Soc.***2006**, *128*, 11894-11905.
11. Kleinermanns, K.; Nachtigalloa, D.; de Vries, M. S. Excited state dynamics of DNA bases. *Int. Rev. Phys. Chem.* **2013**, *32*, 308-342.
12. Buchvarov, I.; Wang, Q.; Raytchev, M.; Trifonov, A.; Fiebig, T. Electronic energy delocalization and dissipation in single- and double-stranded DNA. *Proc. Natl. Acad. Sci. U.S.A.* **2007**, *104*, 4794-4797.

13. Pancur, T.; Schwalb, N. K.; Renth, F.; Temps, F. Femtosecond fluorescence up-conversion spectroscopy of adenine and adenosine: experimental evidence for the $\pi\sigma^*$ state? *Chem. Phys*. **2005**, *313*, 199-212.

14. Gustavsson, T.; Improta, R.; Markovitsi, D. DNA/RNA: Building blocks of life under UV irradiation. *J. Phys. Chem. Lett*. **2010**, *1,* 2025-2030.

15. Kwok, W-M.; Ma, C.; Phillips, D. L. A doorway state leads to photostability or triplet photodamage in thymine DNA. *J. Am. Chem. Soc.* **2008**, *130*, 5131-5139.

16. Yarasi, S.; Ng, S.; Loppnow, G. R. Initial excited-state structural dynamics of uracil from resonance Raman spectroscopy are different from those of thymine (5-methyluracil). *J. Phys. Chem. B* **2009**, *113*, 14336-14342.

17. Yarasi, S.; Brost, P.; Loppnow, G. R. Initial excited-state structural dynamics of thymine are coincident with the expected photochemical dynamics. *J. Phys. Chem. A* **2007**, *111*, 5130-5135.

18. Billinghurst, B. E; Oladepo, S. A; Loppnow, G. R. Initial excited-state structural dynamics of thymine derivatives. *J. Phys. Chem. B* **2012**, *116*, 10496-10503.

19. Billinghurst , B. E.; Yeung, R.; Loppnow, G. R. Excited-state structural dynamics of 5-fluorouracil. *J. Phys. Chem. B* **2006**, *110*, 6185-6191.

20. Ng, S.; Teimoory, F.; Loppnow, G. R. Mass-tuned initial excited-state structural dynamics of DNA nucleobases from UV resonance Raman spectroscopy: 5-deuterouracil. *J. Phys. Chem. Lett.* **2011**, *2*, 2362-2365.

21. Teimoory, F.; Loppnow, G. R., Initial Excited-State Structural Dynamics of 6-Substituted Uracil Derivatives: Femtosecond Angle and Bond Lengthening Dynamics in Pyrimidine Nucleobase Photochemistry. *J. Phys. Chem. A* **2014,** *118* , 12161-12167.

22. El-Yazbi, A. F.; Palech, A.; Loppnow, G. R. Initial Excited-State Structural Dynamics of 2′-Deoxyguanosine Determined via UV Resonance Raman Spectroscopy. *J. Phys. Chem. A* **2011**, 115, 10445-10451.

23. Oladepo, S. A.; Loppnow, G. R. Initial Excited-State Structural Dynamics of 9-Methyladenine from UV Resonance Raman Spectroscopy. *J. Phys. Chem. B* **2011,** *115*, 6149-6156.

24. Onidas, D.; Markovitsi, D.; Marguet, S.; Sharonov, A.; Gustavsson, T. Fluorescence properties of DNA nucleosides and nucleotides: A refined steady-state and femtosecond Investigation. *J. Phys. Chem. B*, **2002**, 106, 11367-11374.

25. Myers, A. B. Excited Electronic State Properties from Ground-State Resonance Raman Intensities. In *Laser Techniques in Chemistry*; Myers, A. B., Rizzo, T. R., Eds.; Wiley: New York, 1995; pp 325-384.

26. Kelley, A. M. Resonance Raman intensity analysis of vibrational and solvent reorganization in photoinduced charge transfer. *J. Phys. Chem. A* **1999**, *103*, 6891-6903.

27. Lee, S.-Y.; Heller, E. J. Time-dependent theory of Raman scattering. *J. Chem. Phys.* **1979**, *71*, 4777-4788.

28. Li, B.; Johnson, A. E.; Mukamel, S.; Myers, A. B. The Brownian oscillator model for solvation effects in spontaneous light emission and their relationship to electron transfer. *J. Am. Chem. Soc.* **1994**, *116*, 11039-11047.

29. Mukamel, S. Principles of Nonlinear Optical Spectroscopy; Oxford University Press: New York, 1995.

30. Fodor, S. P. A.; Rava, R. P.; Hays, T. R.; Spiro, T. G. Ultraviolet resonance Raman spectroscopy of the nucleotides with 266-, 240-, 218-, and 200-nm pulsed laser excitation. *J. Am. Chem. Soc.* **1985,** *107*, 1520-1529.

31. Pepino, A. J.; Segarra-Martí, J.; Nenov, A.; Improta, R.; Garavelli, M. Resolving Ultrafast Photoinduced Deactivations in Water-Solvated Pyrimidine Nucleosides. *J. Phys. Chem. Lett.* **2017,** *8*, 1777-1783.

32. Leulliot, N.; Ghomi, M.; Jobic, H.; Bouloussa, O.; Baumruk, V.; Coulombeau, C., Ground State Properties of the Nucleic Acid Constituents Studied by Density Functional Calculations. 2. Comparison between Calculated and Experimental Vibrational Spectra of Uridine and Cytidine. *J. Phys. Chem. B*, **1999**, 103, 10934-10944.

33. Zhu, X-M.; Wang, H-g.; Zheng, X.; Phillips, D. L. Role of ribose in the initial excited state structural dynamics of thymidine in water **solution: A resonance Raman and density functional theory investigation.** *J. Phys. Chem. B* **2008**, *112,* 15828-15836.

34. Kubasek, W. L.; Hudson, B.; Peticolas, W. L. Ultraviolet resonance Raman excitation profiles of nucleic acid bases with excitation from 200 to 300 nanometers. *Proc. Natl. Acad. Sci. U S A.,* **1985**, *82*, 2369-2373.

35. Sasidharanpillai, S.; Loppnow, G. R. Initial excited-state structural dynamics of 5,6-dimethyluracil from resonance Raman spectroscopy. *J. Phys. Chem. A* **2014**, 118, 4680−4687.

36. Loppnow, G. R.; Billinghurst, B. E; Oladepo, S. A. Excited-state structural dynamics of nucleic acids and their components. In *Radiation induced molecular phenomena in nucleic acids,* Shukla, M.K.; Leszczynski, J., Eds.*;* Springer Science + Business media B. V., 2008, 237-263.

37. Gustavsson, T.; Bányász, Á.; Sarkar , N.; Markovitsi, D.; Improta, R. Assessing solvent effects on the singlet excited state lifetime of uracil derivatives: A femtosecond fluorescence upconversion study in alcohols and D_2O. Chem. Phys., **2008**, *350*, 186-192.

38. Yamazaki, S.; Taketsugu, T. Nonradiative deactivation mechanisms of uracil, thymine and 5-fluorouracil: A comparative ab initio study. *J. Phys. Chem. A* **2012**, *116*, 491-503.

39. Hudock, H. R.; Levine, B. G.; Thompson, A. L.; Satzger, H.; Townsend, D. Gador, N.; Ullrich, S.; Stolow, A.; Martınez, T. J. Ab initio molecular dynamics and time-resolved photoelectron spectroscopy of electronically excited uracil and thymine. *J. Phys. Chem. A* **2007**, *111*, 8500-8508.

40. Pecourt, J-M. L.; Peon, J.; Kohler, B. DNA excited-state dynamics: ultrafast internal conversion and vibrational cooling in a series of nucleosides. *J. Am. Chem. Soc.* **2001,** *123,* 10370-10378.